Published in final edited form as:
Eur J Neurosci. 2008 October ; 28(8): 1629–1640. doi:10.1111/j.1460-9568.2008.06453.x.

Hypocretin/orexin preferentially activates caudomedial ventral tegmental area dopamine neurons

Nicole M. Vittoz, **Brooke Schmeichel**, and **Craig W. Berridge**
Psychology Department, University of Wisconsin, Madison, WI 53706, USA

Abstract

The hypocretin/orexin (HCRT) neuropeptide system modulates behavioral state and state-dependent processes via actions on multiple neuromodulatory transmitter systems. Recent studies indicate that HCRT selectively increases dopamine (DA) neurotransmission within the prefrontal cortex (PFC) and the shell subregion of the nucleus accumbens (NAs), but not the core subregion of the nucleus accumbens (NAc). The circuitry underlying the differential actions of HCRT across distinct DA systems is unclear. The current study examined whether HCRT preferentially activates PFC- and NAs-projecting relative to NAc-projecting DA neurons within the VTA. One week after infusion of the retrograde tracer fluorogold (FG) into the medial PFC, NAc or NAs, animals received a ventricular infusion of HCRT-1. Subsequent analyses conducted across the rostral-caudal extent of the VTA determined the degree to which: (i) Fos-immunoreactivity (ir) was observed within tyrosine hydroxylase (TH)-ir neurons; (ii) TH-ir was observed within FG-ir neurons; and (iii) Fos-ir was observed within FG-ir neurons. HCRT significantly increased Fos-ir in VTA DA (TH-ir) neurons, primarily in a restricted population of small-to-medium-sized DA neurons located within the caudomedial VTA. Furthermore, within this region of the VTA, PFC- and NAs-projecting TH-ir neurons were more likely to contain Fos-ir than were NAc-projecting TH-ir neurons. These results provide novel evidence that HCRT selectively activates PFC- and NAs-projecting DA neurons within the VTA, and suggest a potential role for HCRT in PFC- and NAs-dependent cognitive and/or affective processes. Moreover, these and other observations suggest that the dysregulation of HCRT–DA interactions could contribute to cognitive/affective dysfunction associated with a variety of behavioral disorders.

Keywords

dopamine; hypocretin; nucleus accumbens; orexin; prefrontal cortex; ventral tegmental area

Introduction

The hypocretin (HCRT) or orexin neuropeptide system has been implicated in the regulation of behavioral state and state-dependent processes, particularly under high-arousal conditions, such as stress and reward (Berridge & España, 2005; Harris & Aston-Jones, 2006). Dopamine (DA) systems also modulate a variety of behavioral, affective and cognitive processes under similar conditions (for review, see Goldman-Rakic, 1995; Ikemoto & Panksepp, 1999). Thus, it is of interest that HCRT fibers and receptors are present in midbrain DA nuclei (Peyron *et al.*, 1998; Marcus *et al.*, 2001; Fadel & Deutch, 2002; Korotkova *et al.*, 2002, 2003) and, *in vitro*, HCRT excites a subset of ventral tegmental area (VTA), but not substantia nigra (SN), DA neurons (Korotkova *et al.*, 2002,

Correspondence: Dr C. W. Berridge, as above. berridge@wisc.edu.

2003). Importantly, when infused intracerebroventricularly (i.c.v.) or directly into the VTA, HCRT selectively increases DA efflux within the prefrontal cortex (PFC) and not in the core subregion of the nucleus accumbens (NAc; Vittoz & Berridge, 2006). Additional studies further demonstrate that intra-VTA HCRT increases DA efflux within the shell region of the nucleus accumbens (NAs; Harris & Aston-Jones, 2006; Narita *et al.*, 2006). Combined, these observations suggest that HCRT selectively targets a subset of DA projection systems.

The mechanisms involved in the differential activation of DA systems by HCRT are not known. One possibility is that different subpopulations of VTA DA neurons display differential sensitivity to HCRT. Consistent with this, previous studies indicate that PFC-projecting DA neurons located in the caudomedial portion of the VTA display a unique sensitivity to stress (Deutch *et al.*, 1991). These observations led us to hypothesize that HCRT may preferentially activate PFC- and NAs-projecting DA neurons located in the caudomedial VTA.

To address this hypothesis, the current studies first examined the topographical pattern of DA neuronal activation within the VTA following i.c.v. administration of a wake-promoting dose of HCRT-1 (0.5 nmol; España *et al.*, 2001). Neuronal activation was assessed using immunohistochemical visualization of Fos, the protein product of the immediate-early gene *c-fos*. These studies indicated that within tyrosine hydroxylase-immunoreactive (TH-ir) neurons, HCRT-induced Fos-ir was largely restricted to a subpopulation of small-to-medium-sized TH-ir neurons located within the caudomedial VTA. In a subset of cases, the retrograde tracer fluorogold (FG) was infused into the PFC, NAs or NAc prior to HCRT infusion. Within the caudomedial aspect of the VTA, PFC- and NAs-projecting neurons were more likely to contain Fos-ir than were NAc-projecting neurons. Additional triple-label fluorescent analyses confirmed that HCRT selectively activates TH-ir neurons projecting to the PFC or NAs. These results comprise novel evidence that HCRT preferentially targets a subpopulation of VTA DA neurons that are associated with a variety of higher cognitive and affective processes.

Materials and methods

Animals

Adult male Sprague–Dawley rats (300–400 g; Charles River, Wilmington, MA, USA) were housed in pairs for at least 14 days prior to surgery with *ad libitum* access to food and water on an 13 : 11 h light : dark cycle (lights on 07:00 hours).

Surgery

All animals were stereotaxically implanted under halothane anaesthesia with a 26-gage guide cannula (Plastics One, Roanoke, VA, USA) over the lateral ventricle (−1.0A, 1.35L, −1.40V; coordinates in mm from Bregma with the head level). In a subset of animals, FG (Fluorochrome, Denver, CO, USA) was infused into the PFC (+2.9A, 1.0L), NAs (+1.3A, 1.1L) or NAc (+2.0A, 1.4L) contralateral to the i.c.v. cannula (see below). For PFC infusions, pipettes were inserted at an angle of 4–6° from vertical toward midline, and three infusions were made at different dorsal-ventral levels (−2.2, −3.0, −4.2V) to increase coverage. For NAc/NAs infusions, a single infusion was made at −6.3 to 6.8V.

Animals were allowed 7–10 days recovery following surgery. All facilities and procedures were in accordance with the guidelines regarding animal use and care put forth by the National Institutes of Health of the United States, and were supervised and approved by the Institutional Animal Care and Use Committee of the University of Wisconsin.

FG infusions

Iontophoretic FG infusions (2% in saline at 5.0 μA, 15 min, 5-s pulses, 50% duty cycle) were made using single-barrel glass micropipettes (15–22 μm tip diameter; Friedrich and Dimmock, Millville, NJ, USA) as previously described (Valentino *et al.*, 1994; España *et al.*, 2005). Infusions into the left and right hemispheres were counterbalanced.

Experimental procedures

On the day prior to testing, animals were placed in a Plexiglas testing chamber (32 × 32 × 40 cm) housed in a wooden, sound-attenuating outer chamber (see Berridge & Foote, 1996). Holes in the top and front of the outer chamber permitted entry of infusion lines and videotaping of the animal.

On the morning of testing, between 09:00 and 10:00 hours, an infusion needle (Plastics One) was connected to PE20 tubing threaded through a stainless steel spring. An air bubble (approximately 150 nL) was used to separate infusate from water in the PE20 tubing. The needle was then inserted into the cannula and secured with a plastic threaded sleeve, the needle tip extending 2.5 mm beyond the end of the cannula. Infusions (1 μL/min) were made between 11:30 and 14:30 hours using a microprocessor-controlled pump (Harvard Apparatus, South Natick, MA, USA) situated outside the sound-attenuating chamber. Animals received a 2-μL infusion of artificial extracellular fluid (AECF) or 0.5 nmol HCRT-1 (Orexin-A; Bachem, King of Prussia, PA, USA; dissolved in AECF). Locomotor activity, grooming and feeding were subsequently scored to confirm that HCRT infusion had a behaviorally activating effect similar to that described previously (España *et al.*, 2001). Animals were killed approximately 90 min following the infusion.

Histology and immunohistochemistry

All animals were deeply anesthetized with sodium pentobarbital (Abbott Laboratories, North Chicago, IL, USA) and perfused transcardially with 250 mL heparinized saline [1 unit of heparin (SoloPak Laboratories, Elk Grove Village, IL, USA)/mL 0.9% saline] followed by 400 mL of 4% formaldehyde in 0.1 M phosphate buffer (pH 7.4). Brains were removed, stored in 4% formaldehyde overnight and taken through graded sucrose solutions (20–30% sucrose in 0.01 M phosphate buffer, pH 7.4). A tracking mark was made in the right lateral cortex and brainstem, and 30-μm-thick sections were collected into nine series (wells) using a cryostat. Therefore, sections within any single well were separated by 240 μm (i.e. 8 × 30 μm). Sections were then placed in 0.01 M phosphate-buffered saline (PBS; pH 7.4) with 0.1% sodium azide and stored at 4°C with minimized exposure to light to protect FG autofluorescence. Sections containing i.c.v. infusion needle tracks were stained with Neutral Red dye to confirm accurate placement. For confirmation of PFC FG infusion placement, relevant sections were immunohistochemically stained for FG [diaminobenzidine (DAB): brown reaction product]. For differentiation between FG placement in the NAs vs. NAc, relevant sections were double-labeled for substance P (DAB: brown reaction product) and FG (Vectastain Blue).

Three sets of double-label analyses were performed: TH + Fos, FG + Fos and FG + TH. For TH + Fos, sections were first stained for Fos-ir (DAB: brown reaction product), and then stained for TH-ir (Vectastain Blue: blue reaction product). For FG + Fos, sections were first stained for Fos-ir (DAB), and then stained for FG-ir (Vectastain Blue). For FG + TH, sections were first stained for FG-ir (DAB), and then stained for TH-ir (Vectastain Blue).

For immunoperoxidase-based processing, sections were rinsed with 0.3% Triton X-100 in 0.01 M PBS (PBS-TX) or, in the case of Fos, 0.01 M PBS. Sections were then incubated for 20 min in a quench solution containing 0.75% hydrogen peroxide, rinsed again, and

transferred for 30 min to a blocking solution containing 10% normal goat serum (NGS) and 0.01 M PBS-TX, and rinsed a final time. For Fos processing, sections were incubated for 48 h at 4°C with rabbit anti-rat Fos antibody (1 : 30 000; Oncogene, San Diego, CA, USA). For FG processing, sections were incubated for 24 h at 4°C with rabbit anti-FG antibody (1 : 75 000; Chemicon International, Temecula, CA, USA). For substance P processing, sections were incubated for 24 h at 4°C with rabbit anti-substance P antibody (1 : 10 000; Chemicon International). Anti-Fos, anti-FG and anti-substance P primary antibodies were diluted in 0.01 M PBS containing 0.4% NGS. For TH processing, sections were incubated for 24 h at 4°C with rabbit anti-TH antibody (1 : 18 000; Chemicon International) diluted in 0.1 M PBS-TX. After incubation, tissue was rinsed with 0.01 M PBS, and incubated with goat anti-rabbit biotinylated secondary antibody (1 : 200; Vector Laboratories, Burlingame, CA, USA) for 90 min. Tissue was then rinsed with 0.01 M PBS-TX (or, in the case of Fos, 0.01 M PBS), exposed to an avidin-biotin peroxidase complex (ABC complex; Vector Laboratories) for 60 min and rinsed with 0.01 M PBS. Sections were reacted with either DAB (Vector Laboratories) to yield a brown precipitate or Vectastain Blue (Vector Laboratories) to yield a blue/gray precipitate.

In order to visualize cells triple-labeled with Fos-ir, TH-ir and FG, Fos and TH were visualized using immunofluorescence (red and green, respectively) and FG using autofluorescence (yellow). For immunofluorescence-based processing of Fos, sections were first rinsed with 0.01 M PBS, then transferred for 30 min to a blocking solution consisting of 10% normal donkey serum in 0.01 M PBS-TX. Sections were then rinsed and incubated for 48 h at 4°C with rabbit anti-Fos antibody (1 : 7500; Oncogene) diluted in 0.01 M PBS. After incubation, tissue was rinsed with 0.01 M PBS, and incubated with a Cy3-conjugated donkey anti-rabbit antibody (1 : 100; Jackson Immuno-Research, West Grove, PA, USA) for 90 min and then rinsed. After Fos processing, tissue was transferred for 30 min to a blocking solution consisting of 10% NGS in 0.01 M PBS-TX. Sections were then rinsed and incubated for 24 h at 4°C with mouse anti-TH antibody (1 : 10 000; Chemicon International) diluted in 0.1 M PBS-TX. After incubation, tissue was rinsed with 0.01 M PBS-TX, and incubated in FITC-conjugated donkey anti-mouse antibody (1 : 1000; Jackson ImmunoResearch) for 90 min, and then rinsed. UV light was used to visualize FG autofluorescence.

Sections processed with immunoperoxidase techniques were mounted on microscope slides (Fisher Scientific, Itasca, IL, USA), air-dried, dehydrated in graded alcohols (50–100%), cleared for at least 24 h (Histoclear; Fisher Scientific) and coverslipped using DPX mounting medium (BDH Laboratory Supplies, Garden City, NY, USA). Sections processed for immunofluorescence were mounted on microscope slides (Fisher Scientific), air dried and coverslipped with Vectashield Hard Set mounting medium (Vector Laboratories).

Data analyses and photomicrograph production

The number of Fos-ir, TH-ir, retrogradely labeled and double-labeled neurons was counted at 400× magnification using an Olympus BX51 light microscope. FG-ir and TH-ir cells were counted only when they possessed a clearly definable nucleus. All retrograde labeling analyses were conducted in immunoperoxidase-processed tissue on the hemisphere ipsilateral to the FG infusion.

For Fos + TH and Fos + FG double-label analyses, cells were considered double-labeled only when an obvious nucleus containing brown precipitate was contained within a distinct soma containing blue precipitate. For FG + TH double-label analyses, cells were considered double-labeled only when brown precipitate and blue precipitate overlapped in a relatively homogeneous fashion within the same cell. In some FG + TH cases, retrogradely labeled cells were very darkly stained for FG-ir; in these cases, cells were only counted as double-labeled when processes extending from the soma clearly contained blue precipitate (TH-ir).

Previous observations indicate a concentration of PFC-projecting DA neurons as well as HCRT-ir fibers in the caudal VTA (Swanson, 1982; Deutch *et al.*, 1991; Fadel & Deutch, 2002; Garzon & Pickel, 2004). Based on these observations, quantitative analyses were conducted first on the full rostral-caudal extent of VTA, then on rostral vs. caudal divisions of VTA, and finally within those divisions, in medial vs. lateral areas, as indicated in Fig. 1. In sections considered rostral, an elongated third ventricle was visible and the mammillary bodies were not yet completely detached. In sections considered caudal, the medial lemniscus was either flattened along the ventral edge of the brain or was no longer visible as a distinct fiber tract. In each section, one additional area corresponding to a portion of the SNc approximately at a midpoint of the dorsal-ventral extent was analysed. For each animal, five to six sections were included in these analyses; typically two sections (−5.0 to −5.3 mm AP) were combined to form the rostral division of the VTA and three sections for the caudal division (−6.0 to −6.5 mm AP). The area of tissue examined was comparable for rostral vs. caudal analyses. Each set of analyses was performed on one of the nine series of tissue sections collected from each animal. Thus, cell counts generated in these analyses represent approximately 1/9th the number of labeled cells expected to be contained within a given subregion of the VTA.

The number of TH-ir, Fos-ir or FG-ir cells was counted along with the number of double-labeled cells, and these cell counts were summed across all relevant sections and corrected for the number of sections analysed in a given animal. The number of double-labeled cells was then divided by the total number of TH-ir cells (for TH + Fos and FG + TH) or by the total number of FG-ir cells (for FG + Fos and FG + TH) to give a percentage of double-labeled cells. For triple-labeled analyses, the number of neurons simultaneously labeled with FG, TH-ir and Fos-ir was counted within the caudomedial VTA in immunofluorescence-labeled tissue. With the filters used, FG only emits light in the yellow spectrum and this occurs only with UV illumination.

Photomicrographs were acquired using an Axiocam HRc digital camera (Carl Zeiss, Thornwood, NY, USA). All digital images were matched for brightness and contrast using ADOBE PHOTOSHOP 6.0 software and labeled using ADOBE ILLUSTRATOR 10.0 or MICROSOFT PUBLISHER software.

Statistical analyses

For statistical analyses of Fos + TH double-labeling, the number of Fos-ir nuclei and the number and percentage of double-labeled cells were analysed with a one-way ANOVA with treatment group (HCRT-vs. AECF-treated) as a between-subjects factor. For Fos + FG and FG + TH double-labeling and Fos + FG + TH triple-labeling, the number and percentage of double- or triple-labeled cells were analysed using a one-way ANOVA with FG infusion site as a between-subjects factor (three levels: PFC, NAc and NAs). ANOVAs were followed up with Fisher's LSD *post hoc* tests to directly compare infusion sites. For all three double-label combinations, two additional statistical tests of identical design were conducted on large and small subsets of double-labeled cells. In all cases, statistical tests were conducted on the number and percentage of double-labeled cells for the entire VTA, and for medial-rostral, lateral-rostral, medial-caudal and lateral-caudal divisions (see Fig. 1).

Results

General observations

In the current analyses, the distribution of TH-ir was consistent with previous descriptions of DA cell groups (Lindvall *et al.*, 1978; Phillipson, 1979a; Swanson, 1982). Briefly, TH-ir was localized within the periaqueductal gray, VTA (interfascicular nucleus, rostral linear

nucleus raphe, central linear nucleus raphe, paranigral nucleus and parabrachial nucleus), SN and retrorubral area.

Among VTA DA neurons, there exists a clear diversity of cytoarchitectural properties, including cell/nucleus size, with a concentration of smaller DA neurons located in the medial VTA (Phillipson, 1979b; Margolis *et al.*, 2006b). Furthermore, limited evidence suggests that small PFC-projecting DA neurons within the caudomedial VTA may have unique functional properties (Roeper *et al.*, 2003). For these reasons, TH-ir cell counts were divided into two categories of size (small and large) based on the diameter of the cell body and the size/shape of the nucleus (Fig. 2). Measurements were taken from a random sample of 40 cells of each size category from two animals. Cells categorized as large were spherical or triangular in shape with an average diameter of 19 ± 0.27 μm (mean ± SEM), possessing an average nucleus diameter of 10 ± 0.13 μm. Cells categorized as small were spherical (tending to be quite small) or fusiform (small–medium) with an average length of 12 ± 0.21 μm and an average nucleus diameter of 7.5 ± 0.12 μm. Large and small TH-ir cells were interspersed throughout the VTA. Small TH-ir cells outnumbered large TH-ir cells (overall VTA, small = 475 ± 53; large = 230 ± 23; mean ± SEM). This was particularly true for the caudal VTA (rostral VTA: small = 114 ± 16; large = 89 ± 8; caudal VTA: small = 282 ± 24; large = 94 ± 12). In the caudomedial portion of the VTA small TH-ir cells outnumbered large TH-ir cells by more than 4 : 1 (caudomedial, small = 188 ± 18; large = 41 ± 5).

In general, minimal Fos-ir was observed within AECF-treated animals. HCRT significantly increased the number of Fos-ir nuclei within the VTA (310 ± 31) relative to AECF-treated animals (109 ± 40; $F_{1,17} = 14.4$, $P = 0.001$). The magnitude of this effect appeared smaller than that previously observed in other brainstem areas (i.e. locus coeruleus, supramammillary nucleus; see España *et al.*, 2003). Within the SN, very few Fos-ir nuclei were observed (3.3 ± 0.6 after HCRT; 2.2 ± 0.7 after AECF; $F_{1,17} = 0.45$, $P = 0.51$); therefore all subsequent analyses were limited to the VTA.

HCRT-induced increases in Fos-ir in VTA TH-ir neurons

To assess the degree to which HCRT activated VTA DA neurons, the mean number of Fos-ir + TH-ir double-labeled cells was examined (AECF, $n = 6$; HCRT, $n = 13$; Fig. 2). Throughout the entire rostrocaudal extent of the VTA, HCRT resulted in a significant increase in the number ($F_{1,17} = 13.6$, $P = 0.002$; Fig. 3A) and percentage of TH-ir cells containing Fos-ir nuclei ($F_{1,17} = 20.3$, $P < 0.001$). When examined within the quadrants of the VTA as defined in Fig. 1, the most pronounced HCRT-induced increase in number ($F_{1,16} = 11.9$, $P = 0.003$; Fig. 3B) and percentage ($F_{1,16} = 11.3$, $P = 0.004$) of double-labeled (Fos-ir + TH-ir) cells occurred in the caudomedial VTA.

Given the above-reviewed evidence indicating morphological heterogeneity within VTA DA neurons, additional analyses examined the degree to which HCRT-induced increases in Fos-ir occurred within small and large TH-ir neurons (Table 1) within the caudomedial VTA. These analyses indicated that, within the caudomedial VTA, HCRT produced a significant increase in Fos-ir within small TH-ir cells ($F_{1,16} = 14.3$, $P = 0.002$) and not large TH-ir cells ($F_{1,16} = 0.02$, $P = 0.877$; Fig. 3C). These observations demonstrate that HCRT produces a significant activation of VTA DA neurons (as measured by Fos-ir), and that this activation is particularly evident in the subpopulation of small DA neurons in the caudomedial portion of the VTA. As mentioned above, the caudomedial VTA contains more small TH-ir neurons than the other VTA subdivisions. However, when the percentage of small TH-ir containing Fos-ir nuclei was analysed, the only subregion in which the HCRT-induced Fos expression significantly exceeded that of vehicle was in the caudomedial VTA ($F_{1,16} = 8.0$, $P = 0.01$). Thus, after controlling for the number of small TH-ir cells per subregion, the caudomedial subregion is particularly responsive to HCRT.

Across the entire VTA, TH-ir neurons represented a relatively small percentage of cells displaying Fos-ir (14.9 ± 1.4%). Nonetheless, within the caudomedial subregion of the VTA, a substantially larger proportion of Fos-ir neurons were also TH-ir (28.0 ± 1.6%). These results further indicate an enhanced sensitivity to HCRT of DA neurons located within the caudomedial VTA.

Distribution of retrograde tracer within TH-ir and Fos-ir VTA neurons

The above-described analyses indicate that HCRT preferentially activates DA neurons located within the caudomedial VTA. Additional studies were conducted to assess the degree to which TH-ir neurons in this subregion project to the PFC, NAc or NAs, and the degree to which these projection neurons are responsive to HCRT.

In these studies, animals received iontophoretic infusions of FG into the medial PFC, NAc or NAs. In order to achieve maximal distribution of retrograde tracer within the medial PFC, three iontophoretic infusions of FG were made at three different dorsoventral positions in each animal. In general, these infusions targeted the anterior cingulate, prelimbic and, in some cases, infralimbic subfields (Fig. 2D). Using this approach, a large proportion of the medial PFC was filled with retrograde tracer. Single iontophoretic infusions of FG were made into the NAc and NAs (Fig. 2E–G). NAc infusions were centered at a fairly anterior level to minimize diffusion into the shell subregion. For all cases included in the analyses, it is estimated that infusate filled from 40–80% of the target region, with minimal diffusion outside the target regions.

Across all VTA neurons (TH-ir + non-TH-ir), PFC-projecting cells were sparsely distributed throughout the rostral-caudal and medial-lateral extent of the VTA. NAc-projecting neurons were more numerous than PFC-projecting neurons. The majority of NAc-projecting neurons were found in the caudal VTA. The largest number of retrogradely labeled cells was observed following tracer infusion into the NAs, and these were concentrated in the caudomedial VTA. Consistent with previous observations (Fallon & Moore, 1978; Swanson, 1982), minimal retrograde label was observed within the VTA/SNc in the hemisphere contralateral to FG infusion.

Distribution of TH-ir neurons projecting to PFC, NAc or NAs

The number of FG-ir, TH-ir and FG-ir + TH-ir double-labeled cells was counted following FG infusions into the PFC ($n = 6$), NAc ($n = 6$) or NAs ($n = 4$; Fig. 2H; Table 2). From these counts, the percentage of TH-ir neurons double-labeled with FG-ir and the percentage of FG-ir neurons double-labeled with TH-ir (Table 2) were calculated. Across the entire rostrocaudal extent of the VTA, a similar percentage of TH-ir neurons were double-labeled with FG-ir following FG infusions into the PFC, NAc and NAs (PFC, 6.5 ± 2.0%; NAc, 8.3 ± 1.5%; NAs, 7.9 ± 0.5%). The above-described Fos-ir results indicate that HCRT-responsive DA neurons are largely restricted to a subpopulation of small neurons located within the caudomedial VTA. Within this subregion, a significantly greater number ($F_{2,13} = 13.63$; $P < 0.001$) and percentage ($F_{2,13} = 16.13$; $P < 0.001$) of small DA neurons were identified as NAs-projecting than PFC- or NAc-projecting (Table 2).

The percentage of FG-ir neurons that were also TH-ir was calculated to assess the degree to which HCRT-activated projection neurons in the VTA are likely to be DA neurons. Across the entire rostrocaudal extent of the VTA, DA neurons made up more than one-third of the cells retrogradely labeled from the three target regions (44 ± 5% for PFC-projecting; 39 ± 5% for NAc-projecting; 42 ± 2% for NAs-projecting). Within the caudomedial VTA, the percentage of small retrogradely labeled neurons that were also TH-ir was similar across all three groups (Table 2), indicating that a similar proportion of each projection is TH-ir. Thus,

HCRT-activated neurons are equally likely to be DA neurons, regardless of their projection target.

HCRT-induced Fos-ir in PFC-, NAc- and NAs-projecting neurons in the VTA

To assess the degree to which HCRT activates PFC-, NAc- and NAs-projecting VTA neurons, the number of Fos-ir + FG-ir double-labeled cells was examined in animals with retrograde tracer infusions in each of these areas (Fig. 2I). AECF-treated animals (PFC, n = 1; NAc, n = 2) possessed very few Fos-ir nuclei in the VTA, resulting in a very low number of FG-ir ± Fos-ir double-labeled neurons [PFC-projecting, 2.0 (no error); NAc, 0.5 ± 0.5]. Given the limited Fos-ir in AECF-treated animals, we did not examine the effects of AECF in animals with FG infusions into the NAs. The analyses presented below include only HCRT-treated animals (PFC, n = 5; NAc, n = 4; NAs, n = 4).

Across the entire extent of the VTA, HCRT activated a greater number of NAs-projecting VTA neurons than neurons projecting to the other targets ($F_{2,10}$ = 31.12; P < 0.001; Table 3). However, when expressed as a percentage of FG-ir neurons, a comparable level of activation was observed for PFC- and NAs-projecting cells. There was a non-significant trend for a greater percentage of double-labeled PFC- and NAs-projecting cells vs. NAc-projecting cells ($F_{2,10}$ = 1.36, P = 0.30).

The results described above indicate that HCRT-sensitive DA neurons are largely restricted to the caudomedial VTA. Within this subregion, a significantly greater number of NAs-projecting neurons expressed Fos-ir than did PFC- or NAc-projecting neurons ($F_{2,10}$ = 11.13, P = 0.003; Fig. 4A). However, when calculated as a percentage of FG-positive cells within this subregion, PFC-projecting neurons were significantly more likely to be Fos-positive than NAc-projecting neurons ($F_{2,10}$ = 4.90, P = 0.033; Fig. 4A), with NAs-projecting neurons at an intermediate level. When cell size was accounted for in the caudomedial VTA, a consistent pattern was evident that was most pronounced for small projection neurons. Thus, a greater number of small NAs-projecting neurons were Fos-positive compared with neurons projecting elsewhere ($F_{2,10}$ = 8.86, P = 0.006; Fig. 4B). In terms of the percentage of FG-ir cells, however, small PFC-projecting neurons appeared most sensitive to HCRT administration. Although the omnibus test did not prove significant ($F_{2,10}$ = 2.67, P = 0.12), when treated as a planned comparison small PFC-projecting neurons were significantly more likely to contain Fos-ir nuclei than small NAc-projecting neurons (Fig. 4B). These observations indicate that small PFC- and NAs-projecting neurons, particularly those located in the caudomedial VTA, display a greater sensitivity to HCRT than NAc-projecting neurons.

HCRT-induced Fos-ir in PFC-, NAc- and NAs-projecting DA neurons in the caudomedial VTA

To address whether HCRT administration activates DA neurons within the caudomedial VTA with specific projection targets, a triple-labeling approach using fluorescence microscopy was utilized. These analyses revealed only a small number of cells in this subregion that were both immunopositive for Fos and TH and displayed FG autofluorescence (i.e. triple-labeled; Fig. 5). Triple-labeled cells, though rare, were observed in four out of five animals with FG infusions into the PFC and in four out of four animals with FG infusions into the NAs. In contrast, only two out of four of the animals with NAc infusions showed a triple-labeled cell, and in these two cases the edge of the tracer infusion appeared to encroach slightly upon the shell subregion. Within the caudomedial VTA, the number of triple-labeled cells appeared greater in animals with FG infusions into NAs than in the other two groups. Although the omnibus test did not reach significance ($F_{2,10}$ = 3.94, P = 0.055), when treated as a planned comparison, the number of triple-labeled cells was

significantly greater in the NAs group than in the NAc group (Fig. 6). In terms of the percentage of FG-labeled cells, PFC-projecting neurons were significantly more likely to be triple-labeled than either NAc- or NAs-projecting neurons ($F_{2,10} = 7.74$, $P = 0.009$; Fig. 6). Consistent with the brightfield analyses, triple-labeled cells were generally small in size and were invariably contained within the caudomedial VTA. The current observations thus indicate that HCRT preferentially activates small PFC- and NAs-projecting DA neurons relative to NAc-projecting DA neurons within the caudomedial VTA.

Discussion

Previous observations indicate that *in vivo*, HCRT selectively enhances DA release within the PFC and NAs relative to the NAc (Narita *et al.*, 2006; Vittoz & Berridge, 2006). The neural circuitry underlying this selectivity is not clear. One possibility is that, within the VTA, HCRT acts preferentially on a subpopulation of DA neurons that project to the PFC or to the NAs. The current study demonstrates that HCRT administration preferentially activates small DA (TH-ir) neurons located within the caudomedial portion of the VTA, as measured by Fos-ir. To our knowledge, this is the first reported observation that HCRT acts differentially across topographically and morphologically defined subpopulations of VTA DA neurons. Consistent with the above hypothesis, the current results further indicate that HCRT preferentially activates DA neurons that project to the PFC and NAs relative to those projecting to the NAc. It is noteworthy that a number of Fos-ir nuclei were observed that were not contained within TH-ir cell bodies in the VTA. The neurochemical identity of these non-TH-ir neurons is unclear. However, our triple-labeling studies indicated that within the caudomedial VTA, few FG-positive but non-TH-ir neurons were activated by HCRT (i.e. contained Fos-ir nuclei). This suggests that within this VTA subfield, HCRT has a minimal impact on non-TH-ir neurons projecting to the PFC, NAs or NAc. Combined, the current and previous observations indicate that HCRT selectively activates a subpopulation of DA neurons projecting to two important corticolimbic terminal fields: the PFC and the NAs. This in turn suggests a potentially prominent role for HCRT in the behavioral and physiological processes dependent on these systems, including higher cognitive and affective function.

Technical considerations

Infusion volume is a critical variable in the use of retrograde tracers (Ader *et al.*, 1980), in part because the number of retrogradely labeled cells will be sensitive to the volume of tissue filled with a retrograde tracer. The use of percentage calculations of FG-ir labeled cells avoids this confound. Nonetheless, cell counts permit comparison of the distribution of neurons projecting to a given target field across different VTA subdivisions. For the current studies, we attempted to minimize differences in FG infusion size within a given target field. Consistent with this, we observed similar numbers of retrogradely labeled cells in the VTA across animals receiving FG infusions into a given region. An additional potential confound with retrograde tracers is the possible uptake and transport by fibers of passage. However, in the case of FG, this appears to be minimal with iontophoretic application (Pieribone & Aston-Jones, 1988; España *et al.*, 2005; España & Berridge, 2006).

In some analyses, the number of double- and triple-labeled cells counted was low. However, it is important to note that the cell counts reported here reflect the number of labeled cells contained in only one out of nine series of collected tissue sections. Thus, the total number of labeled cells contained within any subregion of the VTA is expected to be approximately nine times higher than that reported. Moreover, these analyses likely undercount the number of labeled neurons within a given section for a number of reasons. First, our FG infusions did not fill entirely a target region. Additionally, cell counts were limited to those cells with a clearly defined nucleus. Although this prevents the double-counting of neurons, it likely

underestimates the number of labeled cells. Further, in the case of the immunofluorescent (triple-label) analyses, these analyses involved the use of images captured in a single focal plane (in contrast with the brightfield analyses) and thus undercounted the number of TH-ir, Fos-ir and FG-containing neurons within a given section. Finally, it is important to note that modest numbers of VTA DA neurons likely collateralize to innervate large regions of cortex (Lindvall *et al.*, 1978). Thus, a limited number of DA neurons may well provide a substantial dopaminergic innervation to a target region. Of relevance, previous studies indicate that less than 5–10% of discharge activity within one hemisphere of the locus coeruleus (e.g. less than 75–150 out of 1500 neurons) is sufficient to maintain bilateral activation of the forebrain as measured by EEG (Berridge *et al.*, 1993). Thus, we believe it is likely that the HCRT-induced activation of VTA DA neurons described in the current study represents a physiologically significant action on DA neurotransmission. Of course, it is possible that lower cell counts observed in this study may also reflect the fact HCRT-induced increases in DA release in the PFC and NAs involve additional mechanisms beyond HCRT-induced activation of DA neurons.

Fos-ir is not a perfect indicator of neuronal activity. However, these observations display a strong relationship with the previously described actions of HCRT on DA neuronal firing rate observed *in vitro* and on DA release observed in *in vivo* microdialysis studies (Korotkova *et al.*, 2003; Narita *et al.*, 2006; Vittoz & Berridge, 2006). Thus, Fos-ir may well reflect HCRT-induced activation of DA neuronal discharge. At the very least, these observations indicate that VTA projection systems targeting functionally distinct circuitry display differential sensitivity in an important plasticity-related gene (Kleim *et al.*, 1996; Swank *et al.*, 1996; Pongrac & Rylett, 1998; Radulovic *et al.*, 1998).

Mechanisms of HCRT-induced excitation of VTA DA neurons

The current studies indicate that HCRT preferentially activates those DA neurons contained within the caudomedial subdivision of the VTA. The receptor subtypes involved in this action remain to be determined. Within the caudal VTA, HCRTr1 and HCRTr2 receptors appear to be distributed fairly ubiquitously (Narita *et al.*, 2006). Furthermore, a majority of VTA DA neurons appear to express both HCRTr1 and HCRTr2 receptors (Korotkova *et al.*, 2003; Narita *et al.*, 2006). Therefore, differential HCRT receptor expression is unlikely to account for the differential actions of HCRT across subpopulations of VTA DA neurons. Interestingly, ultrastructural evidence suggests that very few HCRT terminals within the VTA make direct synaptic contacts with DA neurons (Balcita-Pedicino & Sesack, 2007). It is possible that the DA neurons in the caudomedial VTA that express HCRT-induced Fos-ir may be those that receive direct synaptic connections from HCRT fibers.

A unique subpopulation of DA neurons

There is growing evidence for the existence of multiple DA systems within the VTA and SN that are anatomically, physiologically and functionally distinct. For example, a restricted subset of PFC-projecting DA neurons within the caudomedial VTA is activated by acute stress (Deutch *et al.*, 1991). In addition, a subset of VTA DA neurons is activated by rewarding brain stimulation (Hunt & McGregor, 1998). Notably, although these studies did not explicitly analyse the topographically and morphologically defined subsets of VTA neurons described in the current study, it appears from the published photomicrographs that both stress- and reward-activated DA neurons may be topographically and morphologically similar to HCRT-sensitive DA neurons observed in the current study (i.e. small caudomedial VTA neurons).

Traditionally, electrophysiological studies identified VTA DA neurons by their low firing rate and long-duration action potentials (e.g. Grace & Bunney, 1983; Schultz *et al.*, 1993;

Margolis *et al.*, 2006b). However, recent studies suggest that these physiological properties do not consistently distinguish DA from non-DA projection neurons within the VTA (Margolis *et al*., 2006a,b). Moreover, preliminary *in vitro* evidence indicates that a subpopulation of PFC-projecting DA neurons exists within the caudomedial VTA that are small in size and, due to a fast basal firing rate, have likely been overlooked in previous electrophysiology studies (Roeper *et al.*, 2003). These neurons also exhibit kappa-opioid receptor sensitivity (Margolis *et al.*, 2006a) and a lack of DA autoreceptor control (Roeper *et al*., 2003). Taken together, these observations support the conclusion that, although few in number, the subpopulation of DA neurons activated by HCRT may be physiologically and functionally unique.

Functional implications of HCRT–DA interactions

Within the PFC and the NAs, DA release is more responsive to appetitive and aversive stimuli than is DA release in the NAc (Barrot *et al.*, 1999; Wu *et al.*, 1999). Anatomical evidence indicates that the NAs is more intensively interconnected with limbic circuitry – including the lateral hypothalamus – than the NAc (Kelley, 1999; Zahm, 1999). Functionally, the NAc is postulated to be involved with dorsal striatal motor learning systems, whereas the NAs is involved in the control of consummatory behavior and the attachment of salience to events surrounding reward (see Kelley, 1999). Therefore, HCRT-induced activation of NAs-projecting DA neurons may influence the attachment of salience to stimuli surrounding appetitive or aversive situations (for reviews, see Salamone, 1994; Ikemoto & Panksepp, 1999; Di Chiara, 2002).

Extensive evidence indicates a prominent involvement of the PFC in a diverse array of cognitive, affective and physiological processes associated with appetitive and aversive conditions (e.g. Jentsch *et al.*, 2000; Davidson, 2003). Moreover, acting directly within the PFC, DA plays a critical role in the regulation of these processes (e.g. Goldman-Rakic, 1996). Combined, these observations indicate that HCRT may modulate higher cognitive and affective processes via activation of PFC- and NAs-projecting DA systems.

Summary

The current study indicates that HCRT preferentially activates a subpopulation of small DA neurons located within the caudomedial region of the VTA. Within this circumscribed region, HCRT appears to preferentially activate PFC- and NAs-projecting neurons relative to NAc-projecting DA neurons. These findings suggest that HCRT selectively increases rates of DA neurotransmission within the PFC and NAs in part by preferentially exciting specific subpopulations of DA neurons. In addition, the current observations provide additional evidence for the existence of a functionally unique subpopulation of VTA DA neurons that, until recently, may have been overlooked in electrophysiological studies.

The dysregulation of DA neurotransmission within the PFC and NAs has long been implicated in the pathophysiology of a number of psychiatric disorders (Goldman-Rakic, 1995; Jentsch *et al.*, 2000). When combined with previous neurochemical observations, the current findings indicate that HCRT exerts a prominent and preferential activation of the PFC- and NAs-projecting branches of the DA system. As such, dysregulation of these actions could contribute to the behavioral and cognitive deficits associated with a variety of neuropsychiatric disorders.

Acknowledgments

This work was supported by PHS grants MH62359, DA10681, DA00389, and the University of Wisconsin Graduate School (C.W.B.). We gratefully acknowledge Maria Jesson for her technical assistance.

Abbreviations

AECF	artificial extracellular fluid
DA	dopamine
DAB	diaminobenzidine
FG	Fluorogold
HCRT	hypocretin
ir	immunoreactive
NAc	core subregion of nucleus accumbens
NAs	shell subregion of nucleus accumbens
NGS	normal goat serum
PBS	phosphate-buffered saline
PFC	prefrontal cortex
SN	substantia nigra
TH	tyrosine hydroxylase
VTA	ventral tegmental area

References

Ader JP, Room P, Postema F, Korf J. Bilaterally diverging axon collaterals and contralateral projections from rat locus coeruleus neurons, demonstrated by fluorescent retrograde double labeling and norepinephrine metabolism. J. Neural Transm. 1980; 49:207–208. [PubMed: 6162001]

Balcita-Pedicino JJ, Sesack SR. Orexin axons in the rat ventral tegmental area synapse infrequently onto dopamine and gamma-aminobutyric acid neurons. J. Comp. Neurol. 2007; 503:668–684. [PubMed: 17559101]

Barrot M, Marinelli M, Abrous DN, Rouge-Pont F, Le Moal M, Piazza PV. Functional heterogeneity in dopamine release and in the expression of fos-like proteins within the rat striatal complex. Eur. J. Neurosci. 1999; 11:1155–1166. [PubMed: 10103112]

Berridge, CW.; España, RA. Hypocretin/Orexin in stress and arousal. In: de Lecea, L.; Sutcliffe, JG., editors. Hypocretins: Integrators of Physiological Functions. New York, NY: Springer; 2005. p. 353-367.

Berridge CW, Foote SL. Enhancement of behavioral and electroencephalographic indices of waking following stimulation of noradrenergic beta-receptors within the medial septal region of the basal forebrain. J. Neurosci. 1996; 16:6999–7009. [PubMed: 8824336]

Berridge CW, Page M, Valentino RJ, Foote SL. Effects of locus coeruleus inactivation on forebrain electroencephalographic activity. Neuroscience. 1993; 55:381–393. [PubMed: 8104319]

Davidson RJ. Affective neuroscience and psychophysiology: toward a synthesis. Psychophysiology. 2003; 40:655–665. [PubMed: 14696720]

Deutch AY, Lee MC, Gillham MH, Cameron DA, Goldstein M, Iadarola MJ. Stress selectively increases fos protein in dopamine neurons innervating the prefrontal cortex. Cereb. Cortex. 1991; 1:273–292. [PubMed: 1668366]

Di Chiara G. Nucleus accumbens shell and core dopamine: differential role in behavior and addiction. Behav. Brain Res. 2002; 137:75–114. [PubMed: 12445717]

España RA, Berridge CW. Organization of noradrenergic efferents to arousal-related basal forebrain structures. J. Comp. Neurol. 2006; 496:668–683. [PubMed: 16615125]

España RA, Baldo BA, Kelley AE, Berridge CW. Wake-promoting and sleep-suppressing actions of hypocretin (orexin): basal forebrain sites of action. Neuroscience. 2001; 106:699–715. [PubMed: 11682157]

España RA, Valentino RJ, Berridge CW. Fos immunoreactivity in hypocretin-synthesizing and hypocretin-1 receptor-expressing neurons: effects of diurnal and nocturnal spontaneous waking, stress and hypocretin-1 administration. Neuroscience. 2003; 121:201–217. [PubMed: 12946712]

España RA, Reis KM, Valentino RJ, Berridge CW. Organization of hypocretin/orexin efferents to locus coeruleus and basal forebrain arousal-related structures. J. Comp. Neurol. 2005; 481:160–178. [PubMed: 15562511]

Fadel J, Deutch AY. Anatomical substrates of orexin-dopamine interactions: lateral hypothalamic projections to the ventral tegmental area. Neuroscience. 2002; 111:379–387. [PubMed: 11983323]

Fallon JH, Moore RY. Catecholamine innervation of the basal forebrain. IV. topography of the dopamine projection to the basal forebrain and neostriatum. J. Comp. Neurol. 1978; 180:545–580. [PubMed: 659674]

Garzon M, Pickel VM. Ultrastructural localization of Leu5-enkephalin immunoreactivity in mesocortical neurons and their input terminals in rat ventral tegmental area. Synapse. 2004; 52:38–52. [PubMed: 14755631]

Goldman-Rakic PS. Architecture of the prefrontal cortex and the central executive. Ann. N. Y. Acad. Sci. 1995; 769:71–83. [PubMed: 8595045]

Goldman-Rakic PS. Regional and cellular fractionation of working memory. Proc. Natl. Acad. Sci. U.S.A. 1996; 93:13473–13480. [PubMed: 8942959]

Grace AA, Bunney BS. Intracellular and extracellular electrophysiology of nigral dopaminergic neurons–1. identification and characterization. Neuroscience. 1983; 10:301–315. [PubMed: 6633863]

Harris GC, Aston-Jones G. Arousal and reward: a dichotomy in orexin function. Trends Neurosci. 2006; 29:571–577. [PubMed: 16904760]

Hunt GE, McGregor IS. Rewarding brain stimulation induces only sparse Fos-like immunoreactivity in dopaminergic neurons. Neuroscience. 1998; 83:501–515. [PubMed: 9460758]

Ikemoto S, Panksepp J. The role of nucleus accumbens dopamine in motivated behavior: a unifying interpretation with special reference to reward-seeking. Brain Res. Brain Res. Rev. 1999; 31:6–41. [PubMed: 10611493]

Jentsch JD, Roth RH, Taylor JR. Role for dopamine in the behavioral functions of the prefrontal corticostriatal system: implications for mental disorders and psychotropic drug action. Prog. Brain Res. 2000; 126:433–453. [PubMed: 11105661]

Kelley AE. Functional specificity of ventral striatal compartments in appetitive behaviors. Ann. N. Y. Acad. Sci. 1999; 877:71–90. [PubMed: 10415644]

Kleim JA, Lussnig E, Schwarz ER, Comery TA, Greenough WT. Synaptogenesis and fos expression in the motor cortex of the adult rat after motor skill learning. J. Neurosci. 1996; 16:4529–4535. [PubMed: 8699262]

Korotkova TM, Eriksson KS, Haas HL, Brown RE. Selective excitation of GABAergic neurons in the substantia nigra of the rat by orexin/hypocretin in vitro. Regul. Pept. 2002; 104:83–89. [PubMed: 11830281]

Korotkova TM, Sergeeva OA, Eriksson KS, Haas HL, Brown RE. Excitation of ventral tegmental area dopaminergic and nondopaminergic neurons by orexins/hypocretins. J. Neurosci. 2003; 23:7–11. [PubMed: 12514194]

Lindvall O, Bjorklund A, Divac I. Organization of catecholamine neurons projecting to the frontal cortex in the rat. Brain Res. 1978; 142:1–24. [PubMed: 626911]

Marcus JN, Aschkenasi CJ, Lee CE, Chemelli RM, Saper CB, Yanagisawa M, Elmquist JK. Differential expression of orexin receptors 1 and 2 in the rat brain. J. Comp. Neurol. 2001; 435:6–25. [PubMed: 11370008]

Margolis EB, Lock H, Chefer VI, Shippenberg TS, Hjelmstad GO, Fields HL. {Kappa} opioids selectively control dopaminergic neurons projecting to the prefrontal cortex. Proc. Natl. Acad. Sci. U.S.A. 2006a; 103:2938–2942. [PubMed: 16477003]

Margolis EB, Lock H, Hjelmstad GO, Fields HL. The ventral tegmental area revisited: is there an electrophysiological marker for dopaminergic neurons? J. Physiol. 2006b; 577:907–924. [PubMed: 16959856]

Narita M, Nagumo Y, Hashimoto S, Narita M, Khotib J, Miyatake M, Sakurai T, Yanagisawa M, Nakamachi T, Shioda S, Suzuki T. Direct involvement of orexinergic systems in the activation of the mesolimbic dopamine pathway and related behaviors induced by morphine. J. Neurosci. 2006; 26:398–405. [PubMed: 16407535]

Peyron C, Tighe DK, van den Pol AN, de Lecea L, Heller HC, Sutcliffe JG, Kilduff TS. Neurons containing hypocretin (orexin) project to multiple neuronal systems. J. Neurosci. 1998; 18:9996–10015. [PubMed: 9822755]

Phillipson OT. The cytoarchitecture of the interfascicular nucleus and ventral tegmental area of tsai in the rat. J. Comp. Neurol. 1979a; 187:85–98. [PubMed: 489779]

Phillipson OT. A golgi study of the ventral tegmental area of tsai and interfascicular nucleus in the rat. J. Comp. Neurol. 1979b; 187:99–115. [PubMed: 489780]

Pieribone VA, Aston-Jones G. The iontophoretic application of fluoro-gold for the study of afferents to deep brain nuclei. Brain Res. 1988; 475:259–271. [PubMed: 3214735]

Pongrac JL, Rylett RJ. Molecular mechanisms regulating NGF-mediated enhancement of cholinergic neuronal phenotype: C-fos transactivation of the choline acetyltransferase gene. J. Mol. Neurosci. 1998; 11:79–93. [PubMed: 9826788]

Radulovic J, Kammermeier J, Spiess J. Relationship between fos production and classical fear conditioning: effects of novelty, latent inhibition, and unconditioned stimulus preexposure. J. Neurosci. 1998; 18:7452–7461. [PubMed: 9736664]

Roeper, J.; Liss, B.; Jones, IW. Soc. Neurosci. Abstr. Washington, DC: Society for Neuroscience Abstract Viewer/Itinerary Planner; 2003. Mapping and functional properties of mesoprefrontal dopaminergic neurons in adult mice. 600.8

Salamone JD. The involvement of nucleus accumbens dopamine in appetitive and aversive motivation. Behav. Brain Res. 1994; 61:117–133. [PubMed: 8037860]

Schultz W, Apicella P, Ljungberg T. Responses of monkey dopamine neurons to reward and conditioned stimuli during successive steps of learning a delayed response task. J. Neurosci. 1993; 13:900–913. [PubMed: 8441015]

Swank MW, Ellis AE, Cochran BN. c-fos antisense blocks acquisition and extinction of conditioned taste aversion in mice. Neuroreport. 1996; 7:1866–1870. [PubMed: 8905682]

Swanson LW. The projections of the ventral tegmental area and adjacent regions: a combined fluorescent retrograde tracer and immunofluorescence study in the rat. Brain Res. Bull. 1982; 9:321–353. [PubMed: 6816390]

Swanson, LW. Brain Maps: Structure of the Rat Brain. Amsterdam: Elsevier; 1992.

Valentino RJ, Page ME, Luppi PH, Zhu Y, Van Bockstaele E, Aston-Jones G. Evidence for widespread afferents to barrington's nucleus, a brainstem region rich in corticotropin-releasing hormone neurons. Neuroscience. 1994; 62:125–143. [PubMed: 7816195]

Vittoz NM, Berridge CW. Hypocretin/Orexin selectively increases dopamine efflux within the prefrontal cortex: involvement of the ventral tegmental area. Neuropsychopharmacology. 2006; 31:384–395. [PubMed: 15988471]

Wu YL, Yoshida M, Emoto H, Tanaka M. Psychological stress selectively increases extracellular dopamine in the 'shell', but not in the 'core' of the rat nucleus accumbens: a novel dual-needle probe simultaneous microdialysis study. Neurosci. Lett. 1999; 275:69–72. [PubMed: 10554987]

Zahm DS. Functional-anatomical implications of the nucleus accumbens core and shell subterritories. Ann. N. Y. Acad. Sci. 1999; 877:113–128. [PubMed: 10415646]

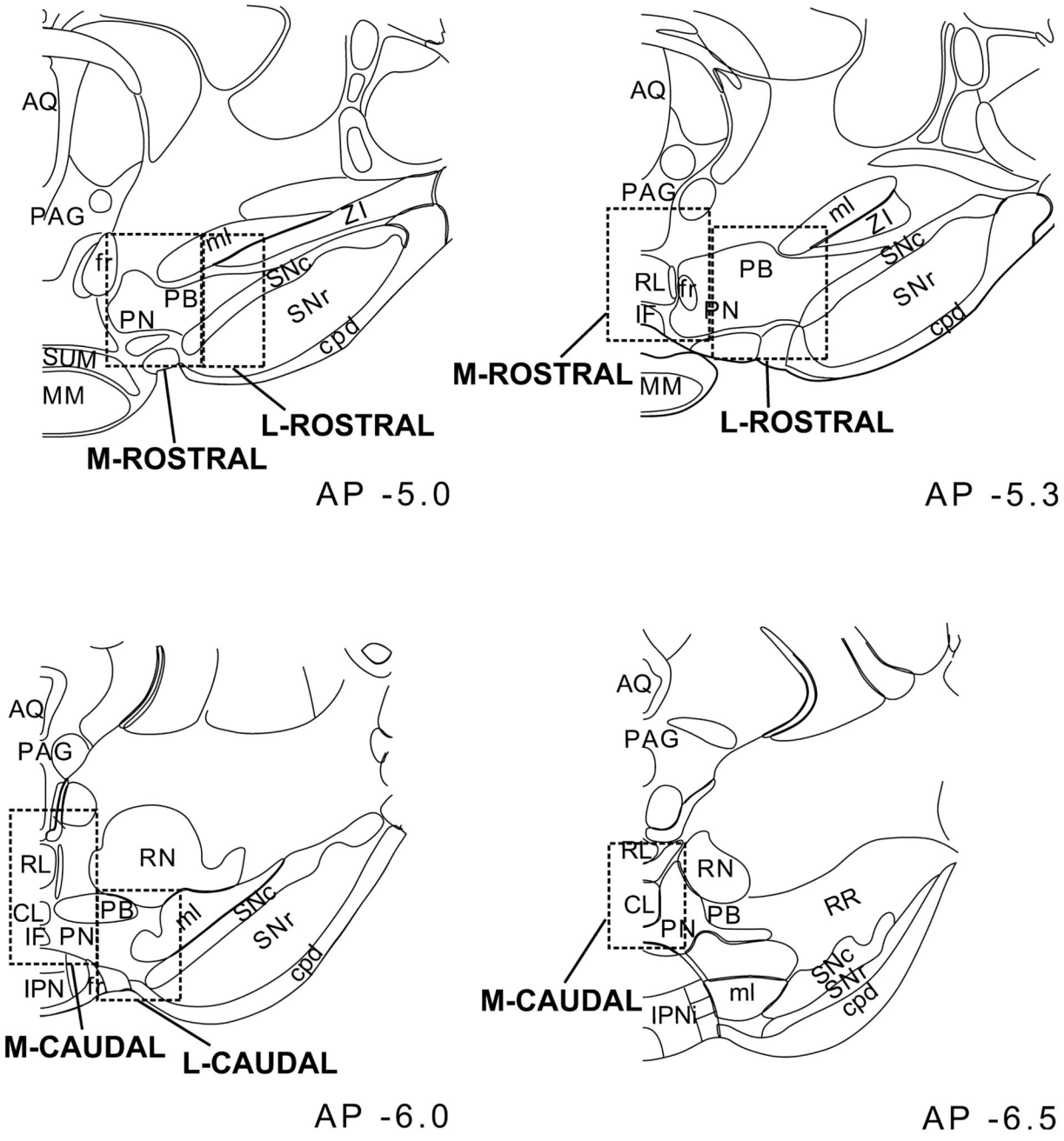

Fig. 1.

Diagram depicting the subregions analysed within rostral (top) and caudal (bottom) levels of the VTA. AP levels are in mm from Bregma. Abbreviations: AQ, cerebral aqueduct; CL, caudal linear nucleus raphé; cpd, cerebral peduncle; fr, fornix; IF, interfascicular nucleus; IPN, interpeduncular nucleus; MM, mammilary bodies; ml, medial lemniscus; PAG, periaqueductal gray; PB, parabrachial nucleus; PN, paranigral nucleus; RL, rostral linear nucleus raphé; RR, retrorubral field; SNc, substantia nigra pars compacta; SNr, substantia nigra pars reticulata; SUM, supramammilary nucleus; ZI, zona incerta. Adapted from Swanson (1992).

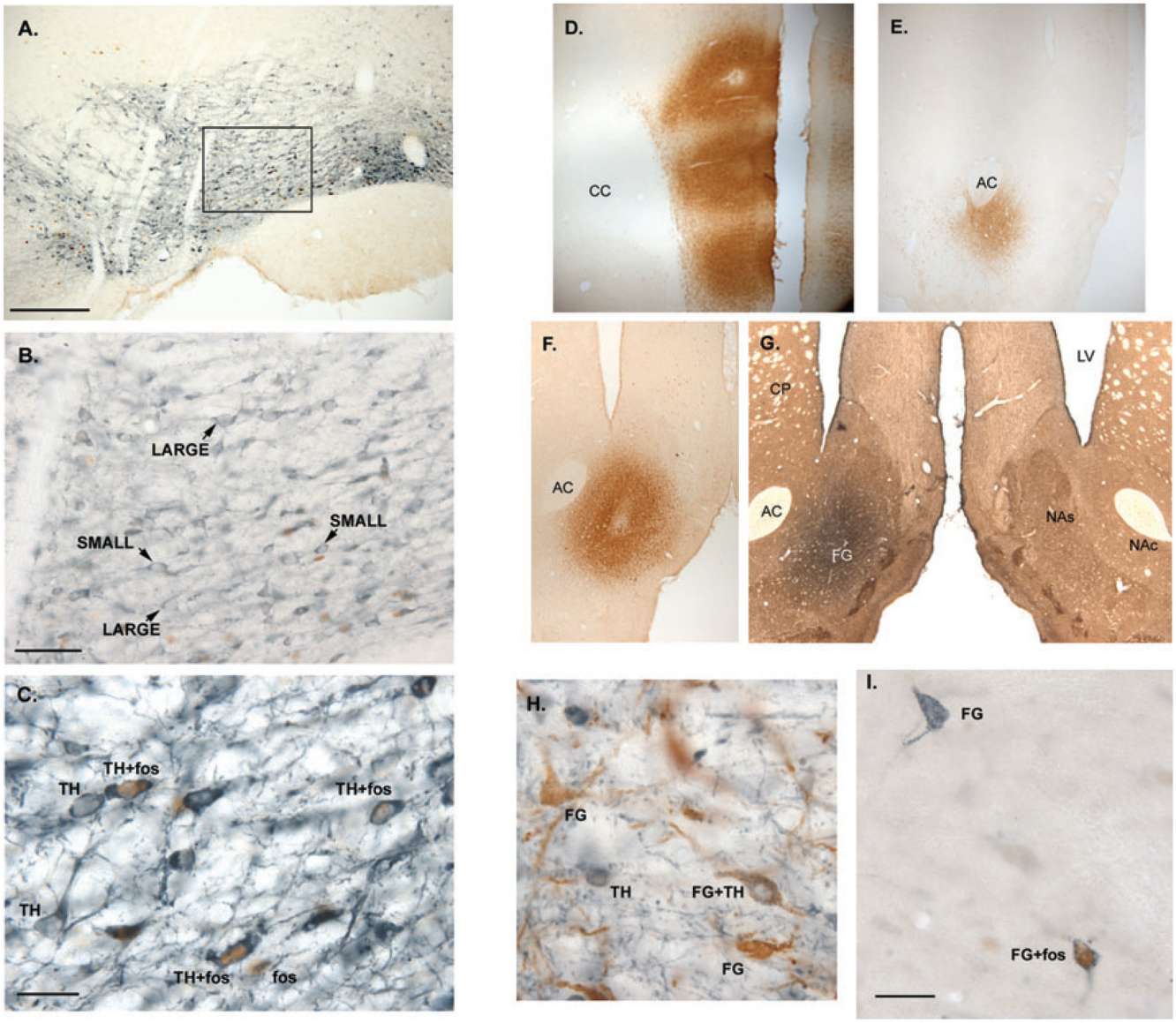

Fig. 2.

Sample photomicrographs depicting tyrosine hydroxylase (TH)-ir + Fos-ir double-labeling (A–C), Fluorogold (FG) infusion sites (D–G), and double-labeling for FG-ir + TH-ir (H) and FG-ir + Fos-ir (I). (A–C) (100×, 400× and 1000×, respectively) Large and small TH-ir neurons (blue) as well as TH-ir + Fos-ir (brown) double-labeling within the caudomedial VTA. (B) Higher-power photomicrograph of the boxed area shown in (A) showing examples of TH-ir neurons categorized as large vs. small. Large and small neurons were intermingled throughout the VTA, with a concentration of small TH-ir neurons in the medial VTA. (C) A separate tissue section containing TH-positive neurons with obvious nuclei, some of which are Fos-positive. (D–F) Example FG infusions (brown) into PFC (40×), NAc (100×) and NAs (100×), respectively, in coronal section. (E) A relatively small FG infusion was placed immediately ventral to the anterior commissure (AC). (G) A photomicrograph of an adjacent section from the same case shown in (F), in which FG-ir was processed with Vector Blue (blue reaction product) and SP-ir was processed with DAB (brown reaction product) as a neuroanatomical marker demarcating NAs vs. NAc. An FG infusion was

placed within the left hemisphere centered in the NAs. The distinction between NAs and NAc is most readily observed in the hemisphere contralateral to the FG infusion. The blue-stained FG largely fills the medial-lateral extent of the NAs and extends approximately two-thirds up the dorsoventral extent. In all cases involving FG infusions into the NAs or NAc, SP-ir was visualized both in sections adjacent to those used to visualize FG-ir alone, and in sections double-labeled for FG-ir + SP-ir. AP levels are in mm from Bregma. Abbreviations: CC, corpus callosum; CP, caudate putamen; LV, lateral ventricle; NAc, nucleus accumbens core; NAs, nucleus accumbens shell. (H–I) 1000× photomicrographs depicting double-labeling for (A) FG-ir (brown) + TH-ir (blue) and (B) FG-ir (blue) + Fos-ir (brown). Scale bars: 300 μm (A), 100 μm (B) and 40 μm (C, H, I).

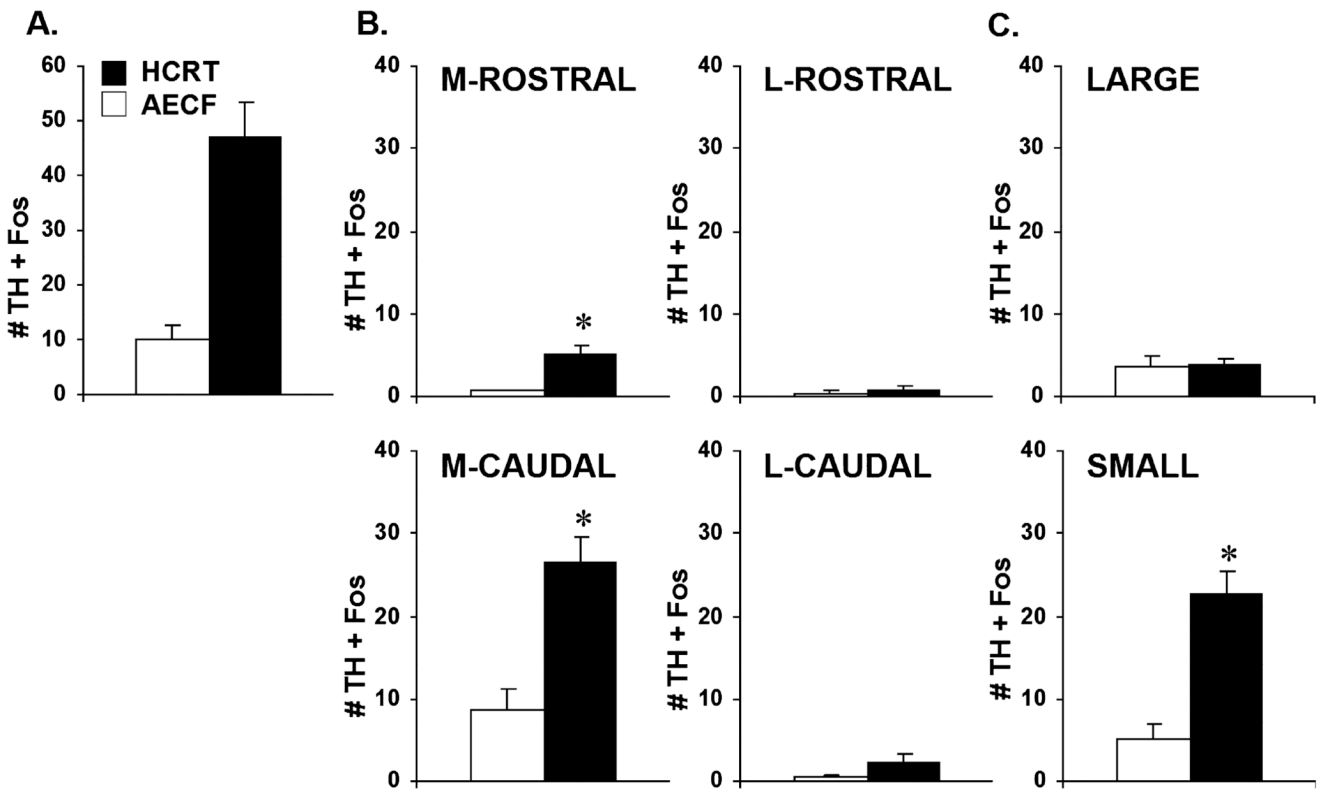

Fig. 3.

The number of tyrosine hydroxylase (TH)-ir neurons that were double-labeled with Fos-ir in the VTA in artificial extracellular fluid (AECF)-treated and hypocretin (HCRT)-treated animals. Presented are the number (mean + SEM) of TH-ir + Fos-ir neurons counted throughout the entire rostrocaudal extent of VTA (A), and within the four VTA subdivisions (B): medial-rostral (M-ROSTRAL); lateral-rostral (L-ROSTRAL); medial-caudal (M-CAUDAL); lateral-caudal (L-CAUDAL). (C) The number of large vs. small TH-ir neurons contained within the caudomedial VTA that were double-labeled for Fos-ir. HCRT produced a robust increase in the number of TH-ir neurons expressing Fos-ir relative to AECF-treated animals (A). The HCRT-induced increase in Fos-ir + TH-ir double-labeling was largely restricted to the caudomedial VTA (M-CAUDAL, B), particularly among small DA neurons (C). *$P < 0.05$.

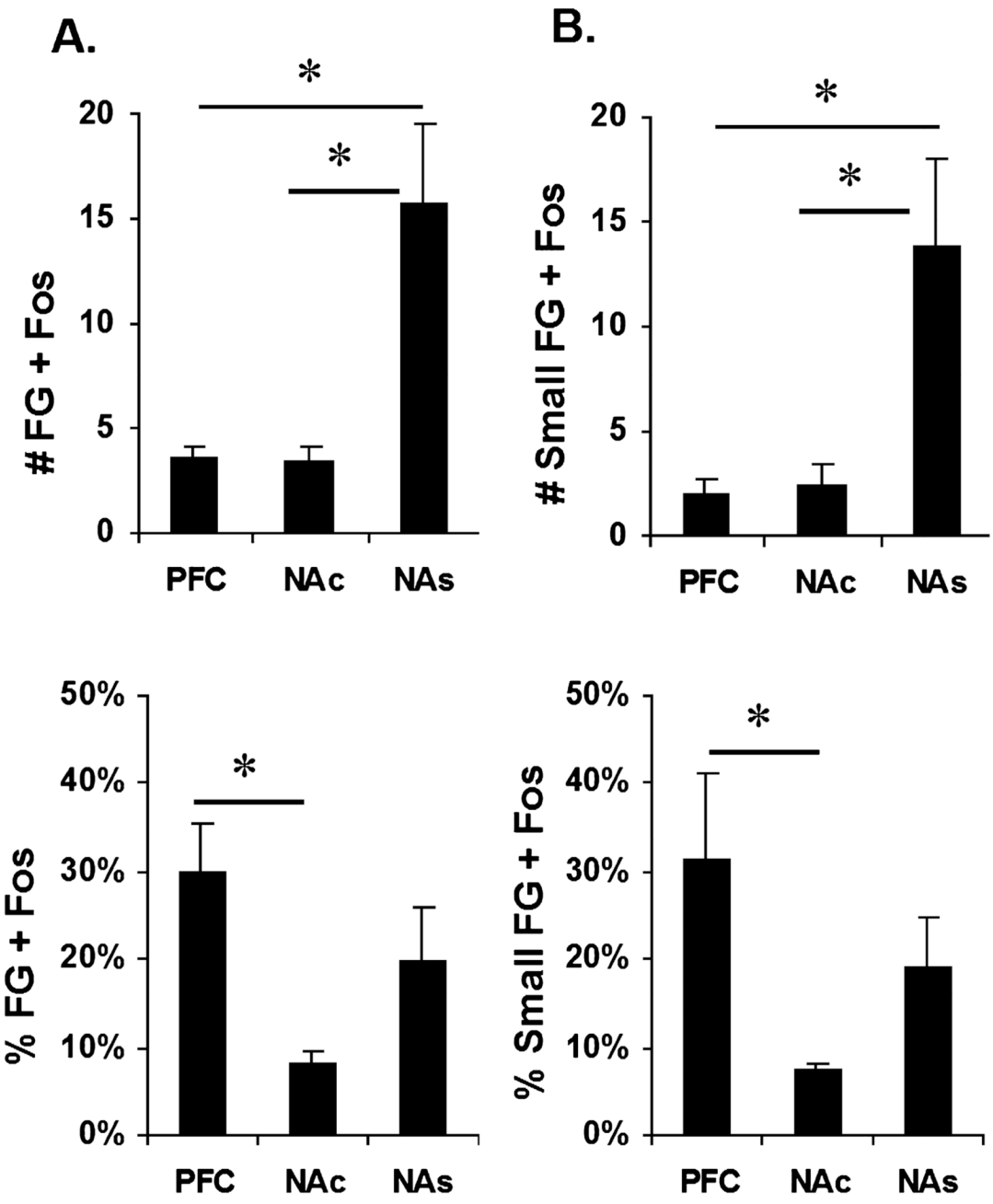

Fig. 4.

The number and percentage of Fluorogold (FG)-ir neurons within the caudomedial VTA double-labeled with Fos-ir, following FG infusions into the prefrontal cortex (PFC), core subregion of nucleus accumbens (NAc) or shell subregion of nucleus accumbens (NAs). Presented are the number (top) and percentage (bottom) of FG-ir + Fos-ir neurons for large + small cells (A) and for small cells only (B). All data are expressed as mean + SEM. Within this region, a greater number of NAs-projecting neurons contained Fos-ir nuclei than did neurons projecting to the other target regions. PFC-projecting neurons were more likely than NAc-projecting neurons to express Fos-ir. *$P < 0.05$.

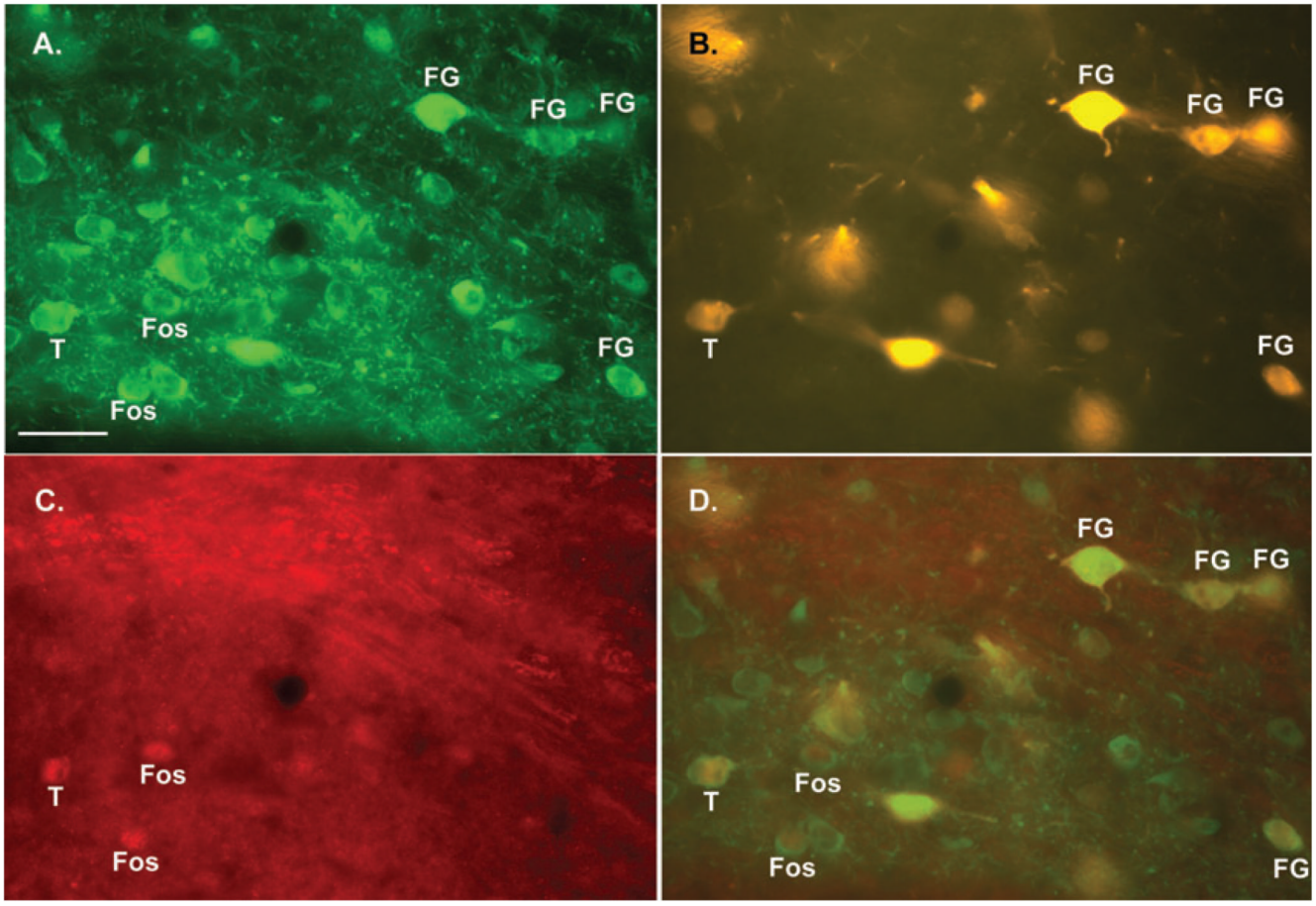

Fig. 5.

Fluorescent photomicrographs depicting retrogradely labeled TH-ir and Fos-ir neurons within the caudomedial VTA. Shown are three photomicrographs from the same field depicting TH-ir (A, green), Fluorogold (FG) autofluorescence (B, yellow) and Fos-ir (C, red). (D) A composite of these three images showing a neuron that was triple-labeled for TH-ir, FG and Fos-ir (T). In all panels, labels indicate TH-ir neurons that were also labeled for FG, Fos-ir or both FG and Fos-ir (T). Magnification is 1000×. Scale bar: 40 μm.

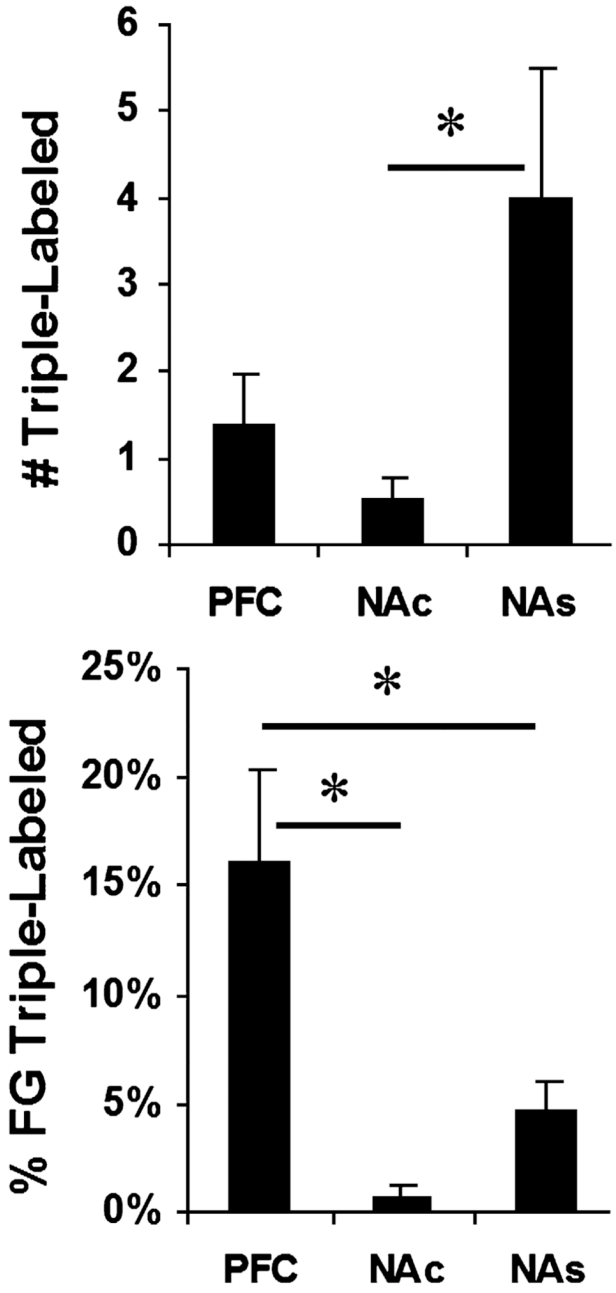

Fig. 6.

The number (top) and percentage (bottom) of retrogradely labeled neurons within the caudomedial VTA that were also labeled for TH-ir and Fos-ir following Fluorogold (FG) infusions into the prefrontal cortex (PFC), core subregion of nucleus accumbens (NAc) or shell subregion of nucleus accumbens (NAs). Data are expressed as mean ± SEM. A greater number of NAs-projecting neurons were triple-labeled than were neurons projecting to the other target regions. However, PFC-projecting neurons were more likely to also express both Fos-ir and TH-ir than were neurons projecting to the other target regions. *$P < 0.05$.

Table 1

TH-ir + Fos-ir double-labeling: cell counts and percentage TH-ir

		VTA division		VTA quadrant				
Treatment	**VTA overall**	**RT**	**CD**	**M RT**	**L RT**	**M CD**	**L CD**	**SN**
Numbers of TH-ir neurons with Fos-ir nuclei								
Large neurons								
AECF	3.1 ± 1.3	0.2 ± 0.2	3.8 ± 1.5	0.0 ± 0.0	0.2 ± 0.2	3.5 ± 1.4	0.2 ± 0.2	0.0 ± 0.0
HCRT	8.6 ± 1.8	1.7 ± 0.6	4.4 ± 0.9	1.5 ± 0.5	0.2 ± 0.1	3.8 ± 0.8	0.5 ± 0.2	0.0 ± 0.0
Small neurons								
AECF	6.9 ± 1.6	1.0 ± 0.4	5.4 ± 1.7	0.7 ± 0.2	0.2 ± 0.2	5.1 ± 1.7	0.2 ± 0.2	0.3 ± 0.3
HCRT	38.4 ± 5.4	4.3 ± 1.0	24.6 ± 3.1	3.6 ± 0.9	0.7 ± 0.3	22.6 ± 2.8	1.8 ± 0.7	0.2 ± 0.1
Percentages of TH-ir neurons with Fos-ir nuclei								
Large neurons								
AECF	1.5 ± 0.6	0.2 ± 0.2	4.3 ± 1.8	0.0 ± 0.0	0.5 ± 0.5	9.4 ± 4.2	0.4 ± 0.4	0.0 ± 0.0
HCRT	3.8 ± 0.5	2.1 ± 0.7	5.0 ± 0.8	5.6 ± 2.2	0.6 ± 0.5	9.6 ± 1.3	1.4 ± 0.7	0.0 ± 0.0
Small neurons								
AECF	2.0 ± 0.5	1.3 ± 0.6	2.1 ± 0.7	2.2 ± 0.8	0.3 ± 0.3	3.0 ± 1.0	0.3 ± 0.3	1.4 ± 1.4
HCRT	7.6 ± 0.8	3.2 ± 0.7	8.8 ± 1.0	6.5 ± 1.4	1.5 ± 0.5	13.0 ± 2.1	2.4 ± 0.9	0.3 ± 0.2

Data are presented as means ± SEM, within the full rostral-caudal extent of the VTA (overall) as well as within rostral (RT) and caudal (CD) divisions. Data are also presented for each of four quadrants within the VTA: medial rostral (M RT), lateral rostral (L RT), medial caudal (M CD) and lateral caudal (L CD), and for a sample area of the SN. Data are shown for AECF-treated (n = 6) and HCRT-treated (n = 13; 0.5 nmol i.c.v.) animals. AECF, artificial extracellular fluid; HCRT, hypocretin; TH, tyrosine hydroxylase; VTA, ventral tegmental area.

Table 2

FG-ir + TH-ir double-labeling: cell count, percentage TH-ir and percentage FG-ir

		VTA division		VTA quadrant			
Infusion site	**VTA overall**	**RT**	**CD**	**M RT**	**L RT**	**M CD**	**L CD**
Numbers of TH-ir neurons co-labeled with FG-ir							
Large neurons							
PFC	17.6 ± 4.8	5.2 ± 2.5	8.5 ± 2.0	2.0 ± 1.4	3.2 ± 1.2	4.0 ± 1.2	4.5 ± 1.2
NAc	22.8 ± 6.7	6.7 ± 2.6	10.8 ± 2.5	4.3 ± 1.4	2.2 ± 1.0	6.1 ± 1.7	4.7 ± 1.3
NAs	7.5 ± 5.6	3.0 ± 1.8	3.5 ± 3.2	2.3 ± 1.3	0.8 ± 0.5	2.3 ± 1.9	1.3 ± 1.3
Small neurons							
PFC	24.5 ± 11.0	4.9 ± 2.0	16.7 ± 8.0	1.7 ± 0.3	3.2 ± 1.8	4.6 ± 1.5	12.2 ± 6.8
NAc	31.8 ± 8.6	6.7 ± 2.1	18.7 ± 5.4	4.2 ± 1.7	2.4 ± 1.0	13.4 ± 3.8	5.2 ± 1.5
NAs	55.4 ± 10.8	8.6 ± 2.9	39.9 ± 7.2	6.0 ± 2.2	2.5 ± 0.9	35.1 ± 7.0	4.0 ± 1.7
Percentages of TH-ir neurons co-labeled with FG-ir							
Large neurons							
PFC	7.1 ± 2.3	6.2 ± 1.7	7.7 ± 3.8	6.2 ± 3.0	8.0 ± 1.8	6.4 ± 3.2	9.5 ± 0.0
NAc	9.2 ± 2.0	7.1 ± 0.8	11.5 ± 4.7	16.7 ± 2.1	4.5 ± 2.9	14.8 ± 2.6	12.4 ± 0.3
NAs	3.5 ± 2.0	3.4 ± 2.3	3.2 ± 3.0	5.0 ± 1.3	2.2 ± 3.7	5.8 ± 1.7	1.7 ± 0.0
Small neurons							
PFC	6.0 ± 1.8	6.7 ± 1.5	5.8 ± 1.3	7.2 ± 2.6	7.7 ± 1.0	2.8 ± 3.2	13.0 ± 0.0
NAc	7.1 ± 2.1	7.5 ± 1.2	6.7 ± 4.2	12.3 ± 2.2	6.1 ± 1.3	7.0 ± 1.5	7.0 ± 0.0
NAs	8.5 ± 0.5	3.5 ± 2.4	11.2 ± 0.8	6.4 ± 0.7	2.1 ± 2.7	16.1 ± 2.6	4.8 ± 0.0
Percentages of FG-ir neurons co-labeled with TH-ir							
Large neurons							
PFC	39.6 ± 3.9	30.0 ± 8.0	47.8 ± 7.4	17.2 ± 8.6	57.1 ± 13.9	34.5 ± 10.0	67.1 ± 9.5
NAc	34.8 ± 5.9	29.3 ± 8.7	39.4 ± 5.4	34.2 ± 9.3	18.6 ± 9.3	37.1 ± 7.2	42.1 ± 5.6
NAs	30.6 ± 10.6	0.0 ± 0.0	22.7 ± 13.2	0.0 ± 0.0	0.0 ± 0.0	22.0 ± 12.9	0.0 ± 0.0
Small neurons							
PFC	48.7 ± 5.6	31.6 ± 5.0	64.3 ± 8.2	19.8 ± 1.2	59.0 ± 16.0	42.5 ± 11.8	73.1 ± 9.2
NAc	40.9 ± 5.0	37.1 ± 6.4	40.7 ± 5.6	42.1 ± 13.7	35.8 ± 11.4	46.5 ± 7.4	36.1 ± 4.9
NAs	44.4 ± 2.4	40.7 ± 7.6	47.3 ± 3.8	39.6 ± 4.3	50.0 ± 17.7	47.0 ± 4.0	46.9 ± 16.3

Data are presented as means ± SEM, within the full rostral-caudal extent of the VTA (overall), as well as within rostral (RT) and caudal (CD) divisions. Data are also presented for each of four quadrants within the VTA: medial rostral (M RT), lateral rostral (L RT), medial caudal (M CD) and lateral caudal (L CD). Data are shown for all animals with satisfactory FG infusions (PFC, *n* = 6; NAc, *n* = 6; NAs, *n* = 4). FG, Fluorogold; NAc, core subregion of nucleus accumbens; NAs, shell subregion of nucleus accumbens; PFC, prefrontal cortex; TH, tyrosine hydroxylase; VTA, ventral tegmental area.

Table 3

FG-ir + Fos-ir double-labeling: cell counts and percentage FG-ir

		VTA division		VTA quadrant			
Infusion site	**VTA overall**	**RT**	**CD**	**M RT**	**L RT**	**M CD**	**L CD**
Numbers of FG-ir neurons with Fos-ir nuclei							
Large neurons							
PFC	4.5 ± 0.9	1.1 ± 0.3	2.6 ± 0.6	1.0 ± 0.4	0.2 ± 0.2	1.6 ± 0.4	0.6 ± 0.3
NAc	3.5 ± 1.4	0.8 ± 0.5	2.3 ± 0.9	0.5 ± 0.5	0.3 ± 0.3	1.0 ± 0.7	1.3 ± 0.6
NAs	3.6 ± 2.2	0.5 ± 0.5	1.8 ± 1.2	0.5 ± 0.5	0.0 ± 0.0	1.8 ± 1.2	0.0 ± 0.0
Small neurons							
PFC	5.6 ± 1.6	2.0 ± 0.9	2.3 ± 0.6	1.6 ± 0.9	0.4 ± 0.2	2.0 ± 0.7	0.2 ± 0.2
NAc	9.2 ± 2.0	3.1 ± 1.1	4.0 ± 1.3	2.8 ± 0.8	0.5 ± 0.5	2.5 ± 0.9	1.5 ± 0.6
NAs	27.3 ± 2.6	3.3 ± 1.1	17.0 ± 3.8	3.3 ± 1.1	0.0 ± 0.0	13.9 ± 4.1	2.8 ± 0.5
Percentages of FG-ir neurons co-labeled with Fos-ir							
Large neurons							
PFC	18.5 ± 5.3	10.1 ± 3.3	28.5 ± 9.9	14.7 ± 6.5	25.0 ± 22.4	30.4 ± 6.2	23.8 ± 19.2
NAc	10.9 ± 3.9	7.9 ± 5.9	13.2 ± 4.6	2.9 ± 2.9	50.0 ± 35.4	6.3 ± 3.8	26.8 ± 11.8
NAs	21.9 ± 9.1	1.6 ± 1.6	28.0 ± 17.3	2.1 ± 2.1	0.0 ± 0.0	40.0 ± 26.5	0.0 ± 0.0
Small neurons							
PFC	22.0 ± 7.0	19.4 ± 8.3	24.0 ± 7.3	20.0 ± 8.2	25.0 ± 12.9	31.3 ± 9.9	4.2 ± 3.7
NAc	12.5 ± 1.9	21.0 ± 4.0	8.4 ± 1.5	43.1 ± 19.2	7.1 ± 7.1	7.5 ± 0.7	11.0 ± 4.5
NAs	23.6 ± 4.6	16.6 ± 5.3	20.6 ± 5.3	20.4 ± 5.4	0.0 ± 0.0	18.9 ± 5.8	37.5 ± 13.8

Data are presented as means ± SEM, within the full rostral-caudal extent of the VTA (overall) as well as within rostral (RT) and caudal (CD) divisions. Data are also presented for each of four quadrants within the VTA: medial rostral (M RT), lateral rostral (L RT), medial caudal (M CD) and lateral caudal (L CD). Data are shown for HCRT-treated (0.5 nmol i.c.v.) animals with satisfactory FG infusions (PFC, $n = 5$; NAc, $n = 4$; NAs, $n = 4$). FG, Fluorogold; NAc, core subregion of nucleus accumbens; NAs, shell subregion of nucleus accumbens; PFC, prefrontal cortex; VTA, ventral tegmental area.